SCUOLA DI INGEGNERIA INDUSTRIALE
E DELL'INFORMAZIONE

EXECUTIVE SUMMARY OF THE THESIS

Time-Optimal Guidance and Control for Spacecraft Interception in LEO

LAUREA MAGISTRALE IN AUTOMATION AND CONTROL ENGINEERING

Author: RICCARDO MARINÒ

Advisor: PROF. ANDREA COLAGROSSI

Academic year: 2025-2026

1. Introduction

Rendezvous and Proximity Operations (RPO) have increasingly evolved from fully cooperative docking missions into strategic, time-critical maneuvers in a congested and contested Low Earth Orbit (LEO). Unlike classical cooperative docking, where fuel minimization and passive safety are the primary focus, defense-oriented or rapid-response interception missions introduce a strict need for time minimization. In non-cooperative engagements, spacecraft must intercept targets rapidly under severe operational constraints, such as hard thrust saturation, limited fuel budgets and navigation uncertainty.

Existing literature often addresses trajectory optimization using Model Predictive Control (MPC) frameworks; running these solvers continuously in real-time is computationally demanding. Consequently, the central motivation of this work is to formulate an efficient, hybrid Guidance and Control architecture. The proposed strategy decouples the control task into a quasiconvex control and trajectory optimization layer based on Relative Orbital Elements (ROE) that is run only a few discrete times based on mission events (such as sensor handover) rather than continuously and combines it with a robust nonlinear tracking layer. This design ensures a globally optimal minimum-time interception while maintaining structural robustness against disturbances and unmodeled errors.

2. Relative Motion Dynamics

To successfully decouple long-term optimal guidance from short-range tracking, this thesis utilizes two distinct formulations for relative motion dynamics.

2.1. Clohessy-Wiltshire (CW) Equations

The Clohessy-Wiltshire (CW) equations [1] provide a linear time-invariant (LTI) state-space representation in the Cartesian Hill (RTN) reference frame. Assuming a circular reference orbit and a small relative separation distance, the decoupled motion in the Cross-Track (z) direction and the coupled motion in the Radial (x) and Along-Track (y) directions are described by the following linear differential equations:

$$\begin{cases} \ddot{x} - 2n\dot{y} - 3n^2 x = u_x, \\ \ddot{y} + 2n\dot{x} = u_y, \\ \ddot{z} + n^2 z = u_z, \end{cases}$$

where $n = \sqrt{\mu/a^3}$ is the target's mean motion and u_x, u_y, u_z are the control accelerations. Expressed in continuous state-space form $\dot{\boldsymbol{x}} = A_{CW}\boldsymbol{x} + B_{CW}\boldsymbol{u}$ with state vector $\boldsymbol{x} = [x, y, z, \dot{x}, \dot{y}, \dot{z}]^\top$ and control vector $\boldsymbol{u} = [u_x \;\; u_y \;\; u_z]^\top$, the system matrices are:

$$A_{CW} = \begin{bmatrix} 0 & 0 & 0 & 1 & 0 & 0 \\ 0 & 0 & 0 & 0 & 1 & 0 \\ 0 & 0 & 0 & 0 & 0 & 1 \\ 3n^2 & 0 & 0 & 0 & 2n & 0 \\ 0 & 0 & 0 & -2n & 0 & 0 \\ 0 & 0 & -n^2 & 0 & 0 & 0 \end{bmatrix},$$

$$B_{CW} = \begin{bmatrix} 0_{3\times3} \\ I_{3\times3} \end{bmatrix}$$

2.2. Relative Orbital Elements (ROE)

For trajectory generation across operational horizons, the quasi-nonsingular Relative Orbital Elements (ROE) formulation is employed. This formulation tracks the geometric differences between the chaser's and the target's orbits. For near-circular target orbits, the state vector $\delta\boldsymbol{\alpha}$:

$$\delta\boldsymbol{\alpha} = \begin{bmatrix} \delta a \\ \delta\lambda \\ \delta e_x \\ \delta e_y \\ \delta i_x \\ \delta i_y \end{bmatrix} = \begin{bmatrix} (a_c - a_t)/a_t \\ (\lambda_c - \lambda_t) + (\Omega_c - \Omega_t)\cos i_t \\ e_c \cos\omega_c - e_t \cos\omega_t \\ e_c \sin\omega_c - e_t \sin\omega_t \\ i_c - i_t \\ (\Omega_c - \Omega_t)\sin i_t \end{bmatrix}$$

The continuous state-space form reads:

$$\delta\dot{\boldsymbol{\alpha}} = A_{ROE}\delta\boldsymbol{\alpha} + B_{ROE}(\tilde{u})\boldsymbol{u}$$

For unperturbed Keplerian motion, the state matrix A_{ROE} is constant and sparse:

$$A_{ROE} = \begin{bmatrix} 0 & \mathbf{0}_{1\times5} \\ -1.5n & \mathbf{0}_{1\times5} \\ \mathbf{0}_{4\times1} & \mathbf{0}_{4\times5} \end{bmatrix}$$

The input matrix $B_{ROE}(\tilde{u})$ is parameterized by the instantaneous mean argument of latitude $\tilde{u}$.

$$\mathbf{B}_{ROE}(\tilde{u}) = \frac{1}{na}\begin{bmatrix} 0 & 2 & 0 \\ -2 & 0 & 0 \\ \sin\tilde{u} & 2\cos\tilde{u} & 0 \\ -\cos\tilde{u} & 2\sin\tilde{u} & 0 \\ 0 & 0 & \cos\tilde{u} \\ 0 & 0 & \sin\tilde{u} \end{bmatrix}$$

Performing trajectory optimization directly within this geometric space significantly reduces artificial secular drift errors inherent in standard Cartesian models.

3. Hybrid Control System Design

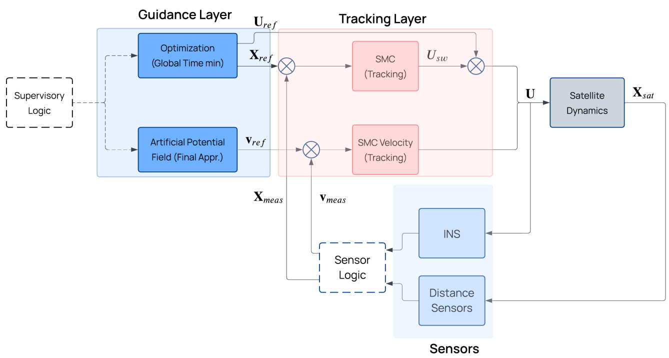

Figure 1: Hybrid Control Architecture Diagram.

In the proposed hybrid GNC architecture, illustrated in Fig. 1, the control system is divided into two primary layers, while the navigation relies on an INS during the far-range phase and relative distance sensors during the close-range phase. The architecture is structured as follows:

- **Guidance Layer:** Operates in two distinct modes. During the rendezvous and proximity phases, an Optimization module generates a full optimal reference state $\mathbf{x}_{ref}$ and a feedforward control $\mathbf{U}_{ref}$. During the final approach, an Artificial Potential Field (APF) module takes over to generate a collision-free velocity reference $\mathbf{v}_{ref}$.
- **Tracking Layer:** Employs two Sliding Mode Controllers (SMC). The Trajectory Tracking SMC follows $\mathbf{x}_{ref}$ by combining the optimal feedforward $\mathbf{U}_{ref}$ with a robust switching term $\mathbf{U}_{sw}$ to compensate for uncertainties. Alternatively, the Velocity Tracking SMC ensures strict adherence to the APF's $\mathbf{v}_{ref}$ during the final meters.
- **Navigation Layer:** Closes the feedback loop via a Sensor Logic module. When the target is out of range $\rho > \rho^*$, it relies on an Inertial Navigation System (INS) that propagates applied controls through an internal dynamic model to estimate the state $\mathbf{x}_{meas}$. Once within range $\rho < \rho^*$, the logic switches to Distance Sensors for direct, accurate relative state measurements.

3.1. Guidance Layer: Quasiconvex Optimal Control

The primary objective of the guidance layer is to minimize the rendezvous time while strictly satisfying fuel and actuator constraints. Because the joint optimization of the control trajectory $\mathbf{u}(t)$ and the final time t_f is non-convex, a bi-level quasiconvex optimization strategy is employed. The free final time formulation can be treated as quasiconvex because, for any fixed t_f, the corresponding feasible set is convex.
The problem is decomposed into two nested loops:

- **Outer Loop (Time Optimization):** A bisection method (Algorithm 1) iterates on t_f to find the minimum horizon for which the problem remains feasible.
- **Inner Loop (Convex Optimization):** For a fixed t_f, the problem is posed as a convex trajectory tracking problem.

This strategy guarantees convergence to the global minimum time T_{opt} due to the exact feasibility detection of the inner convex solver and the monotonicity of the reachable set (i.e., if a maneuver is feasible for time t_a, it is feasible for all $t_b > t_a$).

Algorithm 1 Bisection Optimization Loop

Require: $T_{\text{high}}, T_{\text{low}}$ {Rendezvous time bounds}
Require: $iter$ {Max iterations}

```
tol ← 1, ii ← 0, res ← tol + 1
while ii < iter ∧ res > tol do
    T ← (T_high + T_low)/2
    feas ← ConvexInnerOptimization(T)
    if feas = 1 then
        res ← |T − T_high|
        T_high ← T
    else
        res ← |T − T_low|
        T_low ← T
    end if
    ii ← ii + 1
end while
```

For the inner fixed-time problem, the cost function minimizes the weighted state error. To ensure the optimization remains convex, the physical constraints of the spacecraft are simplified. Specifically, the non-linear physics of fuel depletion are managed by bounding the L_1-norm of the control accelerations to an equivalent maximum velocity increment ($\Delta V_{\max}$). Furthermore, to avoid non-convex, time-varying thrust limits caused by mass loss, the maximum actuator authority ($u_{\max}$) is conservatively fixed as a constant based on the spacecraft's initial mass. The formal Bolza representation is defined as:

$$\min_{\mathbf{u}(\cdot)} \ J = \int_{t_0}^{t_f} \delta\boldsymbol{\alpha}(\tau)^{\mathrm{T}} \mathbf{Q}\, \delta\boldsymbol{\alpha}(\tau) d\tau$$

subject to

$$\begin{aligned}
&\delta\dot{\boldsymbol{\alpha}}(t) = \mathbf{A}_{ROE}\delta\boldsymbol{\alpha}(t) + \mathbf{B}_{ROE}(\tilde{u})\mathbf{u}(t) \\
&\delta\boldsymbol{\alpha}(t_0) = \delta\boldsymbol{\alpha}_0, \\
&\|\delta\boldsymbol{\alpha}(t_f) - \delta\boldsymbol{\alpha}_f\|_\infty \le \varepsilon, \\
&|u_i(t)| \le u_{\max}, \quad \forall i \in \{x, y, z\} \\
&\int_{t_0}^{t_f} \|\mathbf{u}(\tau)\|_1 \, d\tau \le \Delta V_{\max}
\end{aligned}$$

where $\Delta V_{\max} = g_0 I_{sp} \ln\left(\frac{m_0}{m_0 - m_{\text{fuel}}}\right)$, here m_0 is the total mass of the chaser at t_0. To enable feasibility detection, the terminal state constraint is enforced with a small tolerance vector $\boldsymbol{\varepsilon}$.

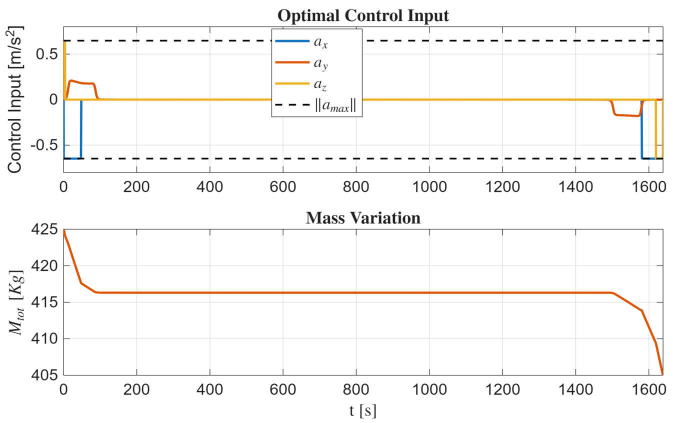

(a) Optimal control acceleration profile

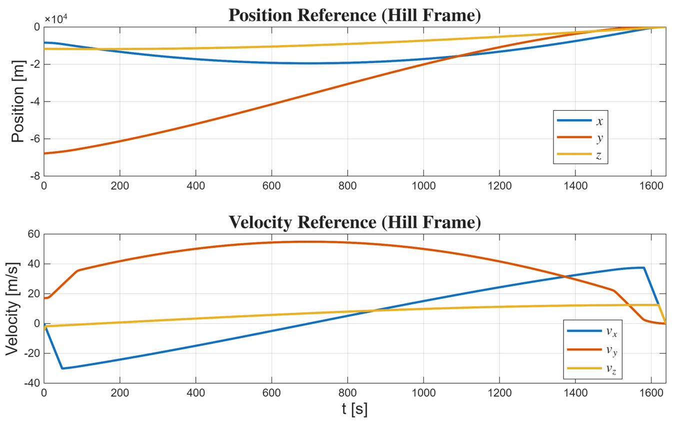

(b) Hill Frame reference position and velocity

Figure 2: Optimal control outputs and generated reference trajectory.

In Fig. 2a, the control profile is shown, where the classical bang-bang structure can be clearly observed. It also illustrates the mass variation computed by the optimal control, showing an estimated consumption of exactly 20 kg of fuel. In Fig. 2b, the generated trajectory is displayed in terms of position and velocity (the optimal control generates a reference in Relative Orbital Elements, which is subsequently transformed into the Cartesian Hill frame).

3.2. Tracking Layer: Sliding Mode Control (SMC)

The Sliding Mode Controller (SMC) serves as the robust tracking layer, ensuring the spacecraft accurately follows the reference trajectory generated by the optimal guidance while rejecting unmodeled perturbations and actuator faults.
The control law combines a feedforward equivalent control $\mathbf{u}_{\text{eq}}$ (provided by the optimal control) with a First-Order quasi-SMC switching term $\mathbf{u}_{\text{sw}}$ designed to mitigate high-frequency chattering:

$$\mathbf{u}_{\text{sw}} = -\eta \tanh(\alpha \boldsymbol{\sigma}) \tag{2}$$

where $\boldsymbol{\sigma}(\mathbf{e}) = \mathbf{C}\mathbf{e}$ is the sliding surface based on the Hill frame state error $\mathbf{e}$, η is the robust switching gain and α adjusts the slope of the hyperbolic tangent.
To simplify tuning and improve tracking performance, the Clohessy-Wiltshire (CW) model is decoupled into in-plane and out-of-plane subsystems. For the in-plane dynamics (x, y), a standard diagonal sliding surface matrix fails to compensate for the Coriolis cross-coupling inherent in the CW equations. Therefore, a modified sliding surface matrix $\mathbf{C}_1$ is formulated, explicitly incorporating off-diagonal terms to cancel the Coriolis effect:

$$\mathbf{C}_1 = \begin{bmatrix} \lambda_x & -2n & 1 & 0 \\ 2n & \lambda_y & 0 & 1 \end{bmatrix}$$

This structural design yields decoupled error dynamics for the in-plane motion, ensuring that control actions on one axis do not perturb the sliding surface of the other:

$$\begin{cases} \dot{\sigma}_x = 3n^2 e_x + \lambda_x e_{\dot{x}} + u_x + d_x \\ \dot{\sigma}_y = \lambda_y e_{\dot{y}} + u_y + d_y \end{cases}$$

Conversely, the out-of-plane motion (z) is naturally decoupled within the linear CW framework, requiring only a straightforward sliding vector $\mathbf{C}_2 = \begin{bmatrix} \lambda_z & 1 \end{bmatrix}$.
Rather than relying on complex manual tuning, the complete set of controller parameters ($[\lambda_x, \lambda_y, \eta, \alpha]$, $[\lambda_z, \eta_z, \alpha]$) are computationally optimized using Particle Swarm Optimization (PSO). This approach navigates the closed-loop stability optimization surface to minimize state tracking errors while penalizing unfeasible control saturation. As illustrated in Fig. 3, the resulting optimally tuned SMC step response shows rapid convergence without overshoot.

3.3. Abort Strategy: E/I Vector Separation

In the event of a critical system failure during the final approach, the guidance objective shifts from interception to collision avoidance. The goal is to establish a passively safe relative orbit around the target using Eccentricity/Inclination (E/I) vector separation [2], guaranteeing a minimum keep-out distance R_{safe} during fault recovery.
To prevent the recovery trajectory from crossing the target, the safe reference state $\delta\boldsymbol{\alpha}_{safe}$ is dynamically determined by the Chaser's instantaneous state at the failure time t_{abort}. The target relative eccentricity ($\delta e_{x,safe}$) and inclination ($\delta i_{x,safe}$) are forced into the same quadrant as the current position to ensure outward expansion:

$$\delta e_{x,safe} = \begin{cases} +\frac{R_{safe}}{a_t} & \text{if } \delta e_x(t_{abort}) \ge 0 \\ -\frac{R_{safe}}{a_t} & \text{if } \delta e_x(t_{abort}) < 0 \end{cases}$$

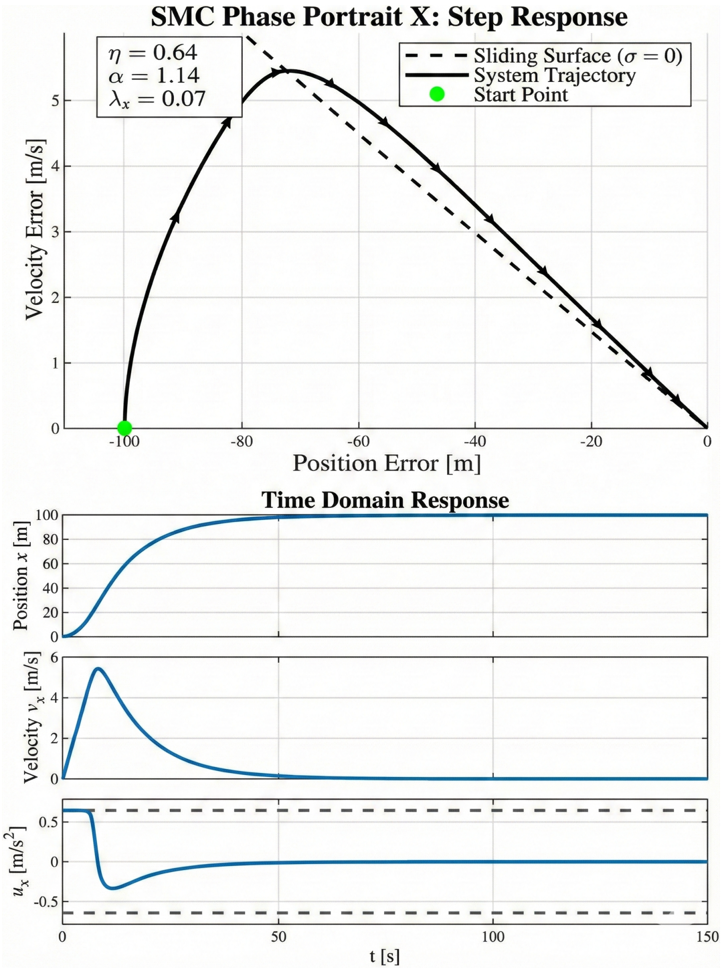

Figure 3: SMC Phase Portrait, SMC step responses for a 100 m initial error on the x-axis. .

$$\delta i_{x,safe} = \begin{cases} +\frac{R_{safe}}{a_t} & \text{if } \delta i_x(t_{abort}) \geq 0 \\ -\frac{R_{safe}}{a_t} & \text{if } \delta i_x(t_{abort}) < 0 \end{cases}$$

For guaranteed passive safety, the relative eccentricity and inclination vectors must be collinear. This alignment ensures that radial and normal oscillations are phased such that they never simultaneously pass through zero:

$$\delta \mathbf{e} \parallel \delta \mathbf{i}$$
$$\Downarrow$$
$$\arctan\left(\frac{\delta e_y}{\delta e_x}\right) = \arctan\left(\frac{\delta i_y}{\delta i_x}\right) + k\pi, \quad k \in \{0, 1\}$$

The guidance strategy trivializes this collinearity requirement by setting ($\delta e_y = \delta i_y = 0$), forcing both vectors to align perfectly along the x-axis.

Finally, to guarantee safety during the transient transfer to the parking orbit, a linear keep-out barrier constraint is embedded within the convex optimization. This mathematically prohibits any inward drift towards the Target while the relative eccentricity is being adjusted:

$$\delta e_x(t) \cdot \text{sgn}(\delta e_x(t_{abort})) \geq |\delta e_x(t_{abort})| \cdot \beta \quad \forall t \in [t_{abort}, t_f]$$

The safety buffer coefficient $\beta \in (0, 1]$ acts as a scaling factor for the KOZ; by reducing β below unity, the constraint is relaxed, allowing the Chaser the necessary flexibility to drift slightly closer to the Target to maintain feasibility or improve maneuver efficiency.

4. Final Approach Strategy

In the critical final approach phase, the guidance shifts from time-optimal interception to strict collision avoidance. The chaser must safely navigate toward the docking point without violating a predefined Keep-Out Zone (KOZ). This is achieved using an Artificial Potential Field (APF) framework, which models the operational space with repulsive obstacles and an attractive target.

4.1. Cardioid-Based KOZ and Cone Corridor

Because the chaser may approach from arbitrary directions, a Cardioid-based potential function adapted from [3] is employed to entirely encapsulate the target within a KOZ. The boundary repulsion term is defined as:

$$h(\boldsymbol{\rho}) = \|\boldsymbol{\rho} + \boldsymbol{\Delta}\|_2^2 + \mathbf{c_s}^\top(\boldsymbol{\rho} + \boldsymbol{\Delta}) - \varphi\|\boldsymbol{\rho} + \boldsymbol{\Delta}\|_2 \tag{3}$$

where $\boldsymbol{\rho} = [x \ y \ z]^\top$ is the relative position vector, $\boldsymbol{\Delta} = [\varrho \ 0 \ 0]^\top$ is a positive offset vector shifting the cardioid along the x-axis and $\mathbf{c_s} = [\varphi \ 0 \ 0]^\top$ scales the cardioid size.

A quadratic attractive potential guiding the chaser toward the target is defined as:

$$N(\boldsymbol{\rho}) = \frac{1}{2}\boldsymbol{\rho}^\top\boldsymbol{\rho} \tag{4}$$

The total potential J_t (shown in Fig. 4a) combines the boundary repulsion term Equation (3) with the quadratic attractive well Equation (4):

$$J_t(\boldsymbol{\rho}) = N(\boldsymbol{\rho})\frac{k_1}{h(\boldsymbol{\rho})} + k_2 N(\boldsymbol{\rho})$$

where k_1 regulates the KOZ boundary steepness and k_2 tunes the attraction toward the target.

To enable the final docking phase, the cardioid potential steers the chaser onto the proper docking axis (the $-x$ direction). Once aligned, the chaser enters a safe geometric approach corridor defined by a Quadratic Cone boundary. This restricts the physical space the spacecraft is allowed to operate in:

$$y^2 + z^2 \leq (x_l \tan\phi_c)^2$$

where $x_l = -x$ represents the local longitudinal frame and ϕ_c is the cone aperture angle.

Inside this safe corridor, a secondary weighted potential function dictates the internal steering logic, strongly prioritizing lateral centering ($k_{lat} \gg 1$) before forward progression:

$$J_{cone}(x_l, y, z) = x_l^2 + k_{lat}(y^2 + z^2)$$

4.2. Velocity-Based Sliding Mode Control

The APF gradient dictates the desired direction of motion, $\mathbf{E_u} = -\nabla J/\|\nabla J\|$, which is subsequently scaled into a reference velocity vector:

$$\mathbf{v}_{ref} = v_{max}\,\mathbf{E_u}$$

To ensure safe docking of the chaser in the final meters, the maximum velocity $v_{\max}$ is adaptively reduced as the relative distance $\|\mathbf{x}\|$ falls below a proximity threshold $\bar{\rho}$:

$$v_{\max} = \begin{cases} v_{\max}, & \text{if } \|\mathbf{x}\| > \bar{\rho} \\ v_{\max}\dfrac{\|\mathbf{x}\|}{\bar{\rho}}, & \text{if } \|\mathbf{x}\| \leq \bar{\rho} \end{cases}$$

A dedicated velocity-tracking SMC ensures robust adherence to this APF gradient reference. By defining the sliding surface proportionally to the velocity error (as proposed in [4]), $\boldsymbol{\sigma} = c\,(\mathbf{v} - \mathbf{v}_{\text{ref}})$, the controller utilizes the same robust control law structure established in Equation (2).

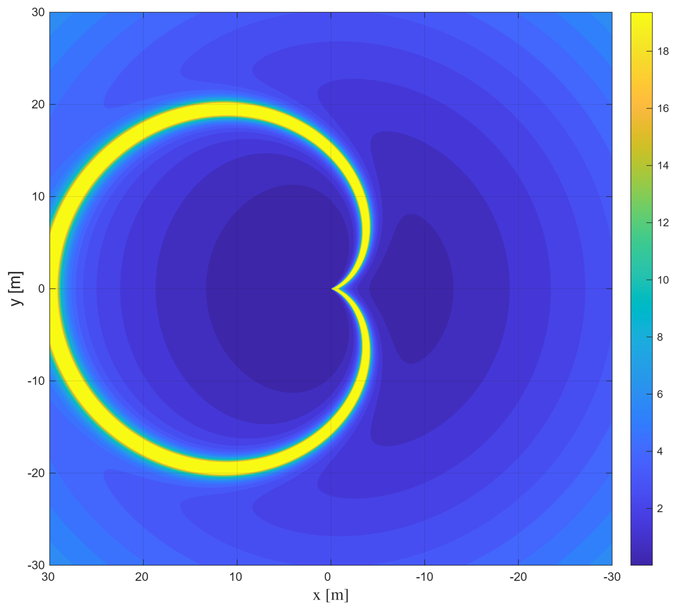

(a) Cardioid potential surface J_t ($z = 0$ slice)

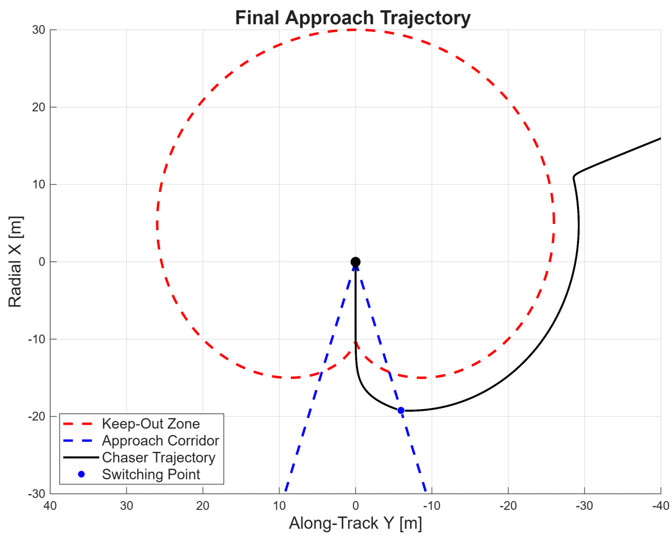

(b) KOZ and Cone approach corridor with an approach trajectory

Figure 4: Cardioid Potential Field and corresponding nominal approach trajectory.

In Fig. 4a, two local minima can be observed: one inside the cardioid (which is theoretically unreachable and therefore not of interest) and one outside, which acts as the global minimum within the operational subspace. Fig. 4b illustrates the resulting Keep-Out Zone and approach cone alongside a simulated final approach trajectory.

5. SMC Parameter Tuning via Particle Swarm Optimization

While the Sliding Mode Controller guarantees robust trajectory tracking, its practical performance is highly sensitive to the selection of its design parameters (sliding surface slopes λ and switching gains η). Determining these optimal parameters analytically is challenging due to hard actuator saturation constraints and non-linear dynamics. Furthermore, classical gradient-based solvers like Sequential Quadratic Programming (SQP) often fail in this context; the numerical integration of stiff dynamics containing discontinuous switching terms generates non-smooth cost landscapes plagued by numerical noise.
To address these challenges, a customized simulation-based Particle Swarm Optimization (PSO) framework is employed to robustly navigate the complex parameter space.

5.1. PSO Update Rules and Topology

$$\begin{aligned} v_{ij}(k+1) &= \chi\Big[v_{ij}(k) + c_1 r_{1j}\left[y_{ij}(k) - x_{ij}(k)\right] \\ &\qquad + c_2 r_{2j}\left[\hat{y}_{ij}(k) - x_{ij}(k)\right]\Big] \\ x_{ij}(k+1) &= x_{ij}(k) + v_{ij}(k+1) \\ \chi &\coloneqq \frac{2}{\left|2 - \phi - \sqrt{\phi^2 - 4\phi}\right|} \end{aligned}$$

where x_{ij} and v_{ij} are the position and velocity of particle i in dimension j, y_{ij} is the particle's personal best position, $\hat{y}_{ij}$ is the neighborhood's local best position, c_1 and c_2 are cognitive and social coefficients, $r_1, r_2 \sim U(0,1)$ are stochastic variables and χ is a scaling factor [5].

5.2. Penalty-Based Cost Function

The optimal parameter set is found by minimizing a custom cost function J_f, which is evaluated by numerically integrating the closed-loop system dynamics at each iteration:

$$\begin{aligned} J_f = &\int_0^T \Big(\mathbf{u}(\tau)^\top R\,\mathbf{u}(\tau) + \mathbf{x}(\tau)^\top Q\,\mathbf{x}(\tau)\Big)\,d\tau \\ &+ k_\phi \int_0^T \phi(\tau)^{n_\phi}\,d\tau \end{aligned}$$

The first part represents an LQR-style performance index, penalizing state tracking errors and control effort via weighting matrices Q, R and $\phi(\tau)$ is a violation function that strictly penalizes control commands attempting to exceed the physical actuator limit $U_{\max}$:

$$\phi(\tau) = \begin{cases} 0, & \text{if } \|\mathbf{u}(\tau)\|_\infty \le U_{\max} \\ \|\mathbf{u}(\tau)\|_\infty - U_{\max}, & \text{if } \|\mathbf{u}(\tau)\|_\infty > U_{\max} \end{cases}$$

Without this penalty, optimization algorithms naturally favor aggressive control laws that demand short, unfeasible high-amplitude spikes. By evaluating the cost function using the ideal (unsaturated) control input while simulating the actual dynamics with saturated inputs, the PSO is heavily penalized for requesting impossible thrusts. This ensures the algorithm reliably converges to physically executable and optimal control gains.

6. Simulations and Results

The proposed hybrid architecture was validated through high-fidelity nonlinear simulations incorporating J_2 gravitational perturbations, atmospheric drag and Inertial Navigation System (INS) drift.

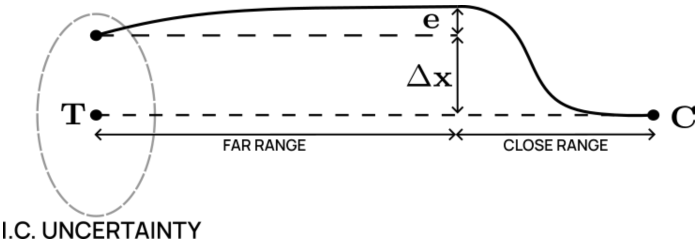

Figure 5: Conceptual schematic of the rendezvous maneuver

6.1. Mission Scenario

The target satellite is the Cosmos 2506 reconnaissance spacecraft operating in a Sun-Synchronous Orbit (SSO). The Chaser is initialized approximately 70 km behind the target, tasked with a time-optimal rendezvous under a strict 20 kg propellant optimization limit.
The absolute orbital parameters of the target and the initial relative Keplerian differences defining the operational scenario are summarized in Table 1.

Target Orbit (Cosmos 2506)			Initial Relative State		
a	7089	km	Δa	-1.2	km
e	$6.017 \cdot 10^{-4}$	-	Δe	0.0008	-
i	98.08	deg	Δi	0.08	deg
Ω, ω, ν	314.6, 250.4, 0	deg	$\Delta\theta$	-0.45	deg

Table 1: Mission Scenario: Target Orbit and Initial Keplerian Differences.

To evaluate the robustness of the system, Monte Carlo simulations introduce an initial position uncertainty reflecting the degradation of Two-Line Element (TLE) data accuracy. The standard deviations for this error distribution in the Hill (RTN) frame are detailed in Table 2.

Initial Position Uncertainty (1σ)		
Radial (σ_R)	500	m
Transverse (σ_T)	800	m
Normal (σ_N)	100	m

Table 2: Standard deviations for the initial position error in the Monte Carlo analysis.

Fig. 5 illustrates the navigation error at the sensor handover time t^* (when the relative distance sensors begin providing direct measurements). The total navigation error is composed of Δx (accounting for linearization errors and target initial position uncertainty) and e_{INS} (the accumulated INS drift). The dashed line represents the optimal reference trajectory; notably, at t_0, the chaser follows a reference path that is inherently shifted by Δx.

6.2. Adaptive vs. Static Guidance Performance

To evaluate mission efficiency, the Monte Carlo analysis compared a static reference tracking strategy (Scenario A) against an adaptive re-optimization strategy (Scenario B).

Scenario A (Static):
The optimal trajectory is computed only once at t_0. Upon sensor handover at 10 km, the SMC is forced to aggressively compensate the accumulated navigation error (Fig. 6). Because the SMC acts as a local feedback controller lacking the look-ahead capability of the optimal control solver, this static tracking strategy is highly inefficient. It results in a mean total **propellant consumption** of 38.2 kg nearly double the allocated budget and a **mean rendezvous time delay** of 40.9 seconds (the additional time required for the SMC to close the position error with respect to the reference at T_{opt}).

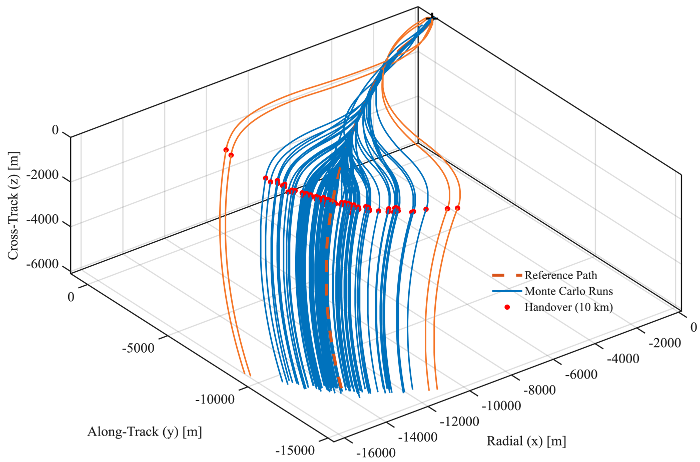

Figure 6: Monte Carlo trajectories (Range < 20 km).

As shown in Fig. 6, worst-case scenarios (orange trajectories) accumulate substantial navigation errors by the handover point. Forcing the spacecraft back to the fixed reference path creates significant instantaneous tracking errors, inducing a transient overshoot of approximately 5% (hundreds of meters). This highlights a fundamental limitation of static guidance: correcting large handover errors demands aggressive control efforts that inevitably lead to trajectory overshoots.

Scenario B (Adaptive):
The supervisory logic triggers a mid-course trajectory re-optimization at the sensor handover. By utilizing the true relative state measured at t^* as the new initial condition for the optimization solver, the Chaser avoids fighting large accumulated navigation errors. This adaptive approach results in a mean total **propellant consumption** of just 23.7 kg (a reduction of approximately 15 kg compared to Scenario A) and drastically minimizes the **mean rendezvous time delay** to only 9.7 seconds.

As shown in Fig. 7, the reference trajectory dynamically updates at the sensor handover time t^*, aligning perfectly with the chaser's state at t^*. By tracking this newly generated reference path, the adaptive strategy completely eliminates the significant control efforts and trajectory overshoots that affect the static approach.

6.3. Final Approach and APF Validation

The Final Approach phase relies on the Cardioid-Cone Artificial Potential Field (APF) to ensure strict collision avoidance. Monte Carlo runs simulated approaches from var-

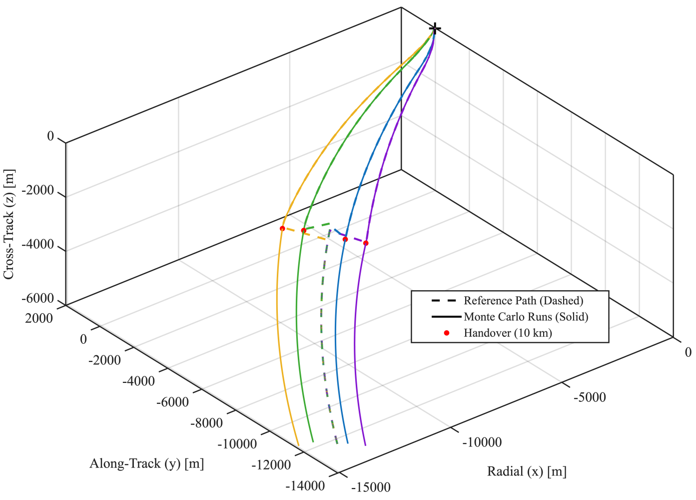

Figure 7: Monte Carlo trajectories (Range < 20 km) for the adaptive strategy. Only a subset of runs is shown to maintain clarity.

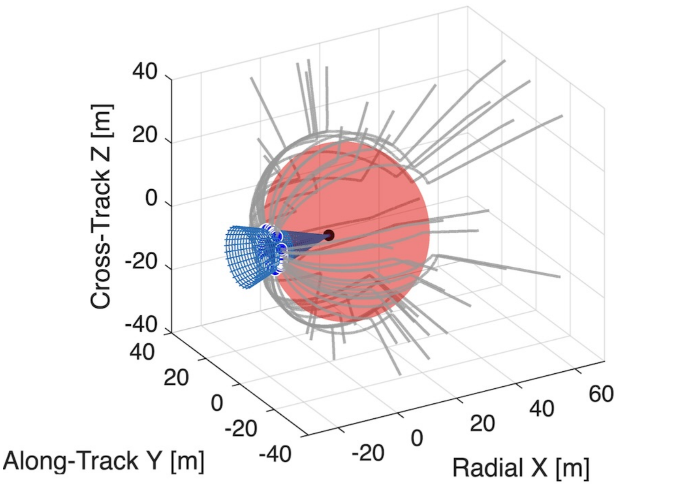

Figure 8: View of the chaser's relative trajectories during the final approach, Monte Carlo simulation for the behind approach.

ious initial states (e.g., frontal and behind the target, as seen in Fig. 8). The APF successfully guided the Chaser to the precise docking port (< 0.1 m relative distance) with a 100% success rate (50/50 runs) without ever breaching the Keep-Out Zone (KOZ). For frontal approaches, the mean time-to-dock was 259.3 s, perfectly aligning with the safety-constrained velocity limits and required an average fuel usage of only 0.71 kg.

6.4. Robustness to Actuator and Sensor Faults

The architecture's robustness was tested against severe hardware faults.

- **Thruster Faults:** Under a "blocked-closed" fault during the maximum acceleration phase, the SMC successfully and autonomously compensated for the total loss of primary actuation, maintaining the spacecraft strictly on the reference trajectory (e.g: Fig. 9 and Fig. 10).
- **Navigation Failure and Abort:** Simulating a critical sensor failure near the KOZ triggered an autonomous time-optimal abort maneuver. The system safely transferred the Chaser into a passive, collision-free elliptical parking orbit in exactly 32 seconds (Fig. 11).

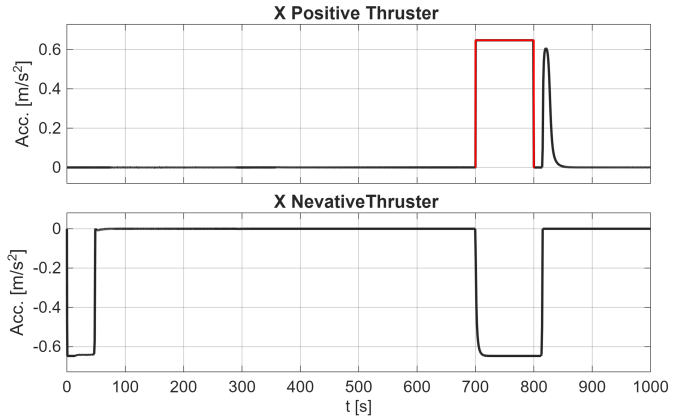

(a) Accelerations generated by the positive and negative X thrusters. The red area indicates the failure.

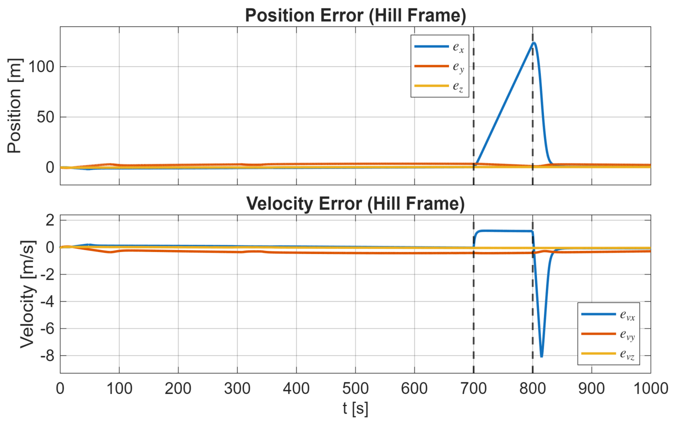

(b) Position error between the reference trajectory and the actual INS measurements. Vertical lines indicate the failure window.

Figure 9: Far-range performance under a positive X-axis stuck-open thruster fault.

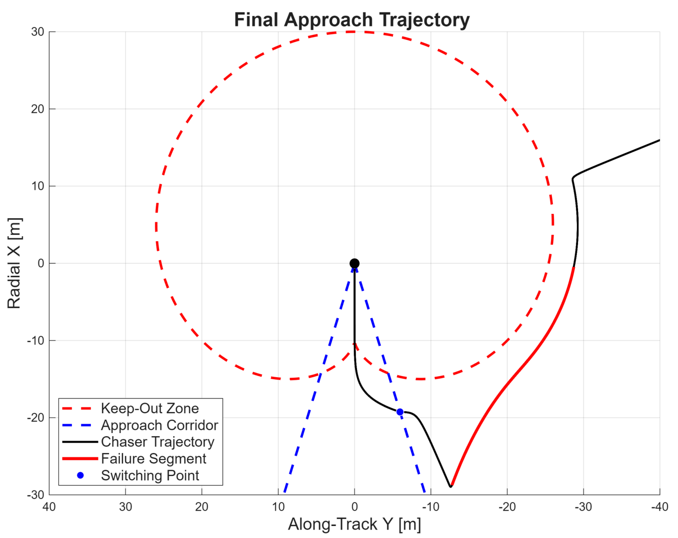

Figure 10: Final approach performance under a negative X-axis stuck-open fault.

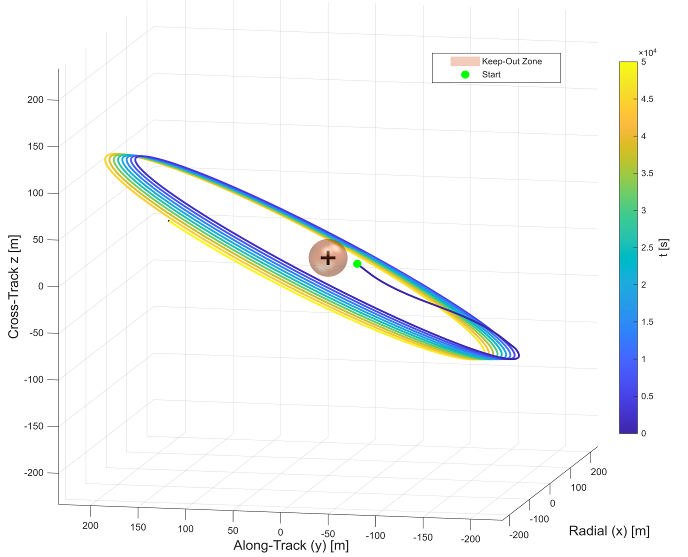

Figure 11: Trajectory showing the transition from the starting point to the safety parking orbit relative to the Target.

7. Conclusions

This thesis has successfully demonstrated the feasibility and high performance of a hybrid architecture specifically designed for time-critical orbital interceptions. By decoupling the problem into a convex optimal Guidance Layer and a robust Sliding Mode Control (SMC) Tracking Layer, the framework achieves both global optimality and disturbance rejection without the high computational costs of real-time optimization solvers.

Closed-loop simulations validated the core contributions of this work:

- **Adaptive Guidance Superiority:** Re-optimizing the trajectory at the sensor handover stage drastically reduces final approach time and propellant consumption by dynamically correcting accumulated open-loop navigation error.
- **Optimized and Robust Tracking:** The PSO-tuned SMC provides exceptional precision, effectively rejecting non-linear environmental perturbations (J_2, atmospheric drag) and maintaining stability under severe actuator faults.
- **Guaranteed Safety and Collision Avoidance:** The Artificial Potential Field (APF) strictly enforces Keep-Out Zone (KOZ) constraints to ensure safe docking from any spatial orientation. Furthermore, the Eccentricity/Inclination (E/I) vector separation strategy guarantees passive safety by autonomously inserting the chaser into a collision-free drift orbit in the event of critical navigation failures.

Ultimately, the proposed architecture provides a comprehensive, modular and automatically tunable GNC framework that is highly adaptable for generic near-circular LEO missions involving non-cooperative targets.

8. Acknowledgements

I would like to thank my advisor, Prof. Andrea Colagrossi, for his guidance and supervision throughout the development of this thesis.

References

[1] WH Clohessy and RS Wiltshire. Terminal guidance system for satellite rendezvous. *Journal of the aerospace sciences*, 27(9):653–658, 1960.

[2] Simone D'Amico and Oliver Montenbruck. Proximity operations of formation-flying spacecraft using an eccentricity/inclination vector separation. *Journal of Guidance, Control, and Dynamics*, 29(3):554–563, 2006.

[3] Qi Li, Jianping Yuan, Bo Zhang, and Huan Wang. Artificial potential field based robust adaptive control for spacecraft rendezvous and docking under motion constraint. *ISA transactions*, 95:173–184, 2019.

[4] Mauro Mancini, Nicoletta Bloise, Elisa Capello, and Elisabetta Punta. Sliding mode control techniques and artificial potential field for dynamic collision avoidance in rendezvous maneuvers. *IEEE Control Systems Letters*, 4(2):313–318, 2019.

[5] Maurice Clerc and James Kennedy. The particle swarm-explosion, stability, and convergence in a multidimensional complex space. *IEEE transactions on Evolutionary Computation*, 6(1):58–73, 2002.

[6] Vincenzo Pesce, Andrea Colagrossi, and Stefano Silvestrini. *Modern spacecraft guidance, navigation, and control: from system modeling to AI and innovative applications.* Elsevier, 2022.